Impact of biogenic emissions of organic matter from a cool-temperate forest on aerosol optical properties

Astrid Müller[a, 1], Kazuma Aoki[b], Eri Tachibana[a], Tsutom Hiura[c], and Yuzo Miyazaki[a, *]

a *Institute of Low Temperature Science, Hokkaido University, Sapporo 060-0819, Japan*

b *Graduate School of Science and Engineering, University of Toyama, Toyama 930-8555, Japan*

c *Field Science Center for Northern Biosphere, Hokkaido University, Sapporo 060-0809, Japan*

* Corresponding Author

Email address: yuzom@lowtem.hokudai.ac.jp (Y. Miyazaki)

[1] Present address: *Center for Global Environmental Research, National Institute for Environmental Studies, 16-2 Onogawa, Tsukuba, Ibaraki 305-8506, Japan*.

Short title: Impact of biogenic organic aerosols on aerosol optical properties

Key words: Biogenic secondary organic aerosols, Aerosol optical properties, Water-soluble aerosols, Sky radiometer

Atmospheric Environment, 229, 117413, https://doi.org/10.1016/j.atmosenv.2020.117413, 2020.

Abstract: Terrestrial biogenic emissions of organic matter can affect the optical properties of atmospheric aerosols and thus impact the radiation budget. To investigate this, the chemical parameters of submicrometer water-soluble aerosols (WSA) collected on filters were compared to optical properties measured by a sky radiometer at a cool-temperate forest site in northern Japan. From June to December, 2015, the WSA samples were collected within the forest canopy, while aerosol optical depth (AOD), single scattering albedo (SSA), absorption Ångström exponent (AAE), and scattering Ångström exponent (SAE) were retrieved above the canopy. The optical properties were compared with the filter-based chemical parameters only when the vertical transport of aerosol particles from the forest canopy to the air above it was significant. The result showed that the AOD and the mass concentrations of WSA exhibited similar and distinct seasonal variations with peaks in summer and autumn. In summer, sulfate accounted for 60% of the mass of WSA, which was linked to a high SSA (> 0.95), low AAE (1.15 ± 0.84), and low SAE (1.25 ± 0.22). In contrast, water-soluble organic matter (WSOM) accounted for 70% of the mass of WSA in autumn. This large fraction of WSOM was associated with a decrease in SSA (0.90–0.95) and an increase in AAE (2.45 ± 0.91) and SAE (1.46 ± 0.15). The results suggest that in summer, aerosol particles with a greater size range corresponded to aerosol chemical compositions dominated by sulfate. In contrast, smaller particles with a strong light absorption at shorter wavelengths, were likely important in autumn and associated with a composition dominated by WSOM. The majority of WSOM in autumn has previously been associated with emissions of α-pinene from the forest floor and the subsequent formation of biogenic secondary organic aerosols (BSOA). This study indicates that α-pinene-derived SOAs, mostly originating from the forest floor, were associated with a summer to autumn decrease in SSA. This process can modulate the radiative effect on a regional scale.

1. Introduction

Atmospheric aerosol particles affect the Earth's radiative forcing directly by absorbing and scattering solar radiation (Ångström, 1964). Light absorption by aerosols is caused mainly by black carbon (BC) and mineral dust (Jacobson, 2001; Ramanathan and Carmichael, 2008). In addition, some fractions of organic carbon (OC) also show light-absorbing properties; these are referred to as brown carbon (BrC) (Andreae and Gelencsér, 2006; Bahadur et al., 2012; Kirchstetter et al., 2004; Moise et al., 2015). Climate models have typically assumed that BC is the only light-absorbing component of aerosols (Kirchstetter et al., 2004) and the effect of light-absorbing OC was generally not considered (Koch et al., 2007). The former assumption may be valid for regions where aerosol particles are dominated by BC (Cazorla et al., 2013). Recent climate models better represent absorbing characteristics of dust and BrC (e.g. Balkanski et al., 2007; Chen et al., 2018; Wang et al., 2014). However, over regions where light absorbing aerosols are dominant, the direct radiative effect (DRE) of OC remains highly uncertain.

Although organic matter accounts for significant fractions of submicrometer aerosols by mass (up to ~90%) (Kanakidou et al., 2005), there are high uncertainties regarding the DRE of biogenic secondary organic aerosols (BSOAs) (Myhre et al., 2013). These include whether or not the effect of BSOAs on the DRE is negative or positive on a regional scale (Andrews et al., 2017). BSOAs in the size of the visible solar spectrum (λ = 380–750 nm) can have an important effect on the DRE (Scott et al., 2014). Scott et al. (2014) estimated that the global annual mean DRE of BSOAs ranged between −0.78 Wm^{-2} and −0.08 Wm^{-2}. Lihavainen et al. (2009) estimated that the regional DRE over a boreal forest in northern Finland ranged from −0.74 Wm^{-2} and −0.37 Wm^{-2} in summer.

77 The wide range of the estimated DREs is largely due to the complex chemical and
78 physical properties, which include the absorbing and scattering, of BSOAs. A negative DRE
79 of BSOAs has been attributed to the latter (Lihavainen et al., 2009; Kim and Paulson, 2013;
80 Scott et al., 2014; Moise et al., 2015, and references therein). The efficiency of light
81 scattering depends on chemical compositions of biogenic volatile organic compounds
82 (BVOCs), their oxidation pathways that lead to the production of BSOAs, the mixing state of
83 BSOA particles, and the time scale of their atmospheric reactions (e.g., Flores et al., 2014;
84 Moise et al., 2015; Nakayama et al., 2010). Most previous studies observed no absorption of
85 solar radiation by BSOAs (Moise et al., 2015, and references therein; Nakayama et al., 2010),
86 or assumed that BSOAs have non-absorbing characteristics (Kim et al., 2010; Kim and
87 Paulson, 2013; Moise et al., 2015). In contrast, other previous studies reported light
88 absorption by organic matter at wavelengths between 350 nm and 470 nm (Andreae and
89 Gelencsér, 2006; Kirchstetter et al., 2004; Lambe et al., 2013; Song et al., 2013; Yang et al.,
90 2009). The gap in current knowledge requires a study to investigate the impact of BSOAs on
91 the DRE in the ambient atmosphere.

92 The strength and types of BVOC emissions depend on vegetation type, phenology, and
93 various meteorological conditions (e.g., Mielonen et al., 2018). Boreal and cool-temperate
94 forests cover the second largest forest area in the world (FAO, 2001). α-pinene is one of the
95 most abundant BVOC in boreal and cool-temperate forests (Guenther et al., 1995; Rinne et
96 al., 2009). Light absorbing properties of BSOA produced from α-pinene have been
97 documented in laboratory experiments (Lambe et al., 2013; Song et al., 2013; Zhong and
98 Jang, 2011). Filter-based off-line measurements of submicrometer water-soluble aerosols
99 (WSA) were made within a canopy of a cool-temperate forest site in northern Japan from
100 June to December 2015. During the same period, ground-based measurements of aerosol
101 optical properties above the forest canopy were simultaneously conducted at the same forest

site. In this study, chemical properties of WSA and the retrieved optical properties were compared to elucidate the effect of the observed BSOA on DRE on a regional scale.

2. Experimental Data and Methods

2.1. Measurement site

Fig. 1 shows the location and surroundings of the observation site in a cool-temperate zone where ambient submicrometer aerosol samples and data on the optical properties of aerosols were obtained simultaneously. The site is Hokkaido University's Tomakomai Experimental Forest (TOEF) (42°43'N, 141°36'E) (Hiura, 2005) located in the southwestern part of Hokkaido, northern Japan. The area of the TOEF is 2715 ha. It is located to the north of urban industrial and port area of Tomakomai city, which faces the Pacific Ocean. The TOEF is classified as a mixed cool-temperate forest consisting of mature and secondary deciduous and planted coniferous trees. Typical naturally occurring species include Mongolian oak (*Quercus crispula*), mono maple (*Acer mono*), Korean whitebeam (*Sorbus alnifolia*), Japanese lime (*Tilia japonica*); planted species include Japanese larch (*Larix leptolepsis*), Sakhalin fir (*Abies sachalinensis*), and Sakhalin spruce (*Picea glehnii*) (*Hiura*, 2005). Also characteristic of this site are various types of forest floor covers (Takafumi and Hiura, 2009) and shallow and less weathered volcanogenic regosols (Shibata et al., 1998).

The meteorological data used in this study were obtained by the Japan Meteorological Agency (http://www.jma.go.jp/jma/indexe.html). In autumn and winter, northerly local wind with local horizontal wind speeds of 3.3 ± 1.4 m s^{-1} were dominant and came from the forested area **(Fig. 1** and **Fig. 2d)**. In contrast, the prevailing southerly wind with speeds of 2.7 ± 0.8 m s^{-1} came from the urban and coastal area were observed in summer. The monthly average temperature from June to December 2015 ranged from 0.9 ± 1.8 °C (December) to 20.8 ± 1.0 °C (August).

2.2. Aerosol sampling and off-line measurements of the chemical parameters

Submicrometer aerosol samples were continuously collected using a high-volume air sampler (HVAS; Model 120SL, Kimoto Electric, Osaka, Japan), deployed at an altitude of ~18 m above the forest floor (Müller et al., 2017). A cascade impactor (CI; Model TE-234, Tisch Environmental, Cleves, OH, USA) attached to the HVAS is used to collect size-segregated particles (Miyazaki et al., 2012) at a flow rate of 1130 L min^{-1}. The filter samples obtained at the bottom stage of the impactor were analyzed, which collects particles with aerodynamic diameter smaller than 0.95 μm. The samples were collected on quartz fiber filters (25 cm × 20 cm) from June to December 2015, with a sampling duration of each aerosol sample being approximately 1 week. To remove contaminants, quartz fiber filters were pre-combusted at 410 °C for 6 hours. The collected filters were stored individually in glass jars with a Teflon-lined screwed cap and were kept frozen at −20 °C until the analysis.

Fifteen aerosol samples were extracted with ultrapure water followed by being filtered through a 0.22−μm pore syringe filter. The extracts were then measured for each chemical parameter. The extracts have been analyzed in terms of their water-soluble organic carbon (WSOC) concentrations (Miyazaki et al., 2014, 2012), which were converted to water-soluble organic matter (WSOM) concentrations using a conversion factor of 1.8 (Finessi et al., 2012; Yttri et al., 2007). Furthermore, the concentrations of major inorganic ions (Cl^-, NO_2^-, NO_3^-, SO_4^{2-}, Ca^{2+}, Mg^{2+}, Na^+, NH_4^+, K^+) were obtained by injecting the extracts into an ion chromatograph (Model 761 compact IC; Metrohm) (Miyazaki et al., 2009). Thus, the fraction of non-sea-salt sulfate was calculated based on the concentrations of sulfate and sodium. Further details about the chemical analysis are given in Müller et al. (2017). In this study, the

149 sum of the mass concentrations of WSOM and inorganic ions measured is defined as water-
150 soluble aerosols (WSA).

151

152 **2.3. Aerosol optical properties**

153 The optical properties of aerosols above the forest canopy were measured using a sky
154 radiometer (POM-02; Prede Co., Ltd., Tokyo, Japan). It was deployed at an altitude of ~30 m
155 above the ground at TOEF as part of the sky radiometer network (Aoki et al., 2008). It
156 measures the direct solar irradiance and diffuse sky radiance at 11 wavelengths every ~10
157 min. Aerosol optical properties were retrieved using 5 wavelengths (0.4, 0.5, 0.675, 0.87, and
158 1.02 μm) (Aoki et al., 2013; Aoki and Fujiyoshi, 2003) by using SKYRAD.pack version 4.2
159 algorithms (Nakajima et al., 1996). The spectral extinction of the solar irradiance at each
160 wavelength by aerosol particle is defined as aerosol optical depth (AOD), which is a measure
161 of aerosol loading in the atmospheric column. Because the maximum radiation intensity of
162 the solar spectrum occurs at wavelength of about 500 nm, AOD at that wavelength is
163 presented in this study as in other previous studies. AOD below 0.2 typically indicates a clear
164 atmosphere, whereas AOD > 0.4 indicates high aerosol loadings such as polluted air (e.g.,
165 Salinas et al., 2013). The Ångström exponent (AE) is a parameter that describes the
166 dependence of AOD on the wavelength of the light (Ångström, 1964), which is a measure of
167 the particle size. With the use of AE, the particle size can be classified into coarse and fine
168 modes (Salinas et al., 2009). For example, AE < 1 indicates that a volume fraction of fine-
169 mode particles is less than 0.5, while larger AE values indicates a larger fractions of fine
170 mode aerosols (Schuster et al., 2006).

171 The single scattering albedo (SSA) is defined as the ratio of scattering to extinction
172 (absorption + scattering) (e.g., Hansen et al., 1997). SSA indicates whether aerosol particles

have radiative warming, or cooling effects which includes effects of surface reflectance (Myhre et al., 2013). SSA > 0.95 represents scattering/reflective aerosols (Lee et al., 2010; Levy et al., 2007), whereas SSA < 0.90 indicates more absorbing aerosols. The mixture of scattering and absorbing aerosols gives SSA values typically between 0.90 and 0.95. The absorption Ångström exponent (AAE) expresses the wavelength dependence of the aerosol light absorption. AAE indicates the dominant chemical composition of light-absorbing aerosols. The size range of these aerosols depends primarily on the scattering Ångström exponent (SAE). AAE and SAE are defined in the spectral dependence of the absorption aerosol optical depth (AAOD) and scattering aerosol optical depth (SAOD), respectively, as follows (Bahadur et al., 2012; Cazorla et al., 2013; Giles et al., 2012; Russell et al., 2010):

$$AAE = -\frac{\ln(AAOD(\lambda_1)/AAOD(\lambda_2))}{\ln(\lambda_1/\lambda_2)} \quad \textbf{(1)}$$

$$SAE = -\frac{\ln(SAOD(\lambda_1)/SAOD(\lambda_2))}{\ln(\lambda_1/\lambda_2)} \quad \textbf{(2)}$$

where

$$AAOD(\lambda) = AOD(\lambda) \times (1 - SSA(\lambda)) \quad \textbf{(3)}$$

$$SAOD(\lambda) = AOD(\lambda) \times SSA(\lambda) \quad \textbf{(4)}$$

Wavelengths of λ_1 = 400 nm and λ_2 = 675 nm used in this study are similar or the same as those used in previous studies (e.g., Bahadur et al., 2012; Cazorla et al., 2013; Russell et al., 2010).

Black carbon (BC) has an AAE value around 1.0 (e.g., Bergstrom et al., 2007; Giles et al., 2012; Russell et al., 2010). Higher AAE values, of 1.5–3.0, indicate a significant contribution from mineral dust (e.g., Bergstrom et al., 2007; Giles et al., 2012; Russell et al.,

2010). AAEs greater or less than 1.0 indicate light-absorbing aerosols coated with either light absorbing or non-absorbing components (Lack and Cappa, 2010). SAEs represent aerosol size ranges and typically have values between 0.0 to 4.0. Higher SAE values (e.g., > 2.0) indicates relatively smaller particles, such as BC or anthropogenic sulfate, while smaller SAE values (e.g., < 2.0) indicates larger particles such as dust, sea salt, or photochemically aged aerosols (Cappa et al., 2016; Cazorla et al., 2013; Schmeisser et al., 2017, and references therein). In this study, the SSA and AAE data are used to discuss the systematic difference in those values among the different seasons, rather than to discuss their absolute values quantitatively. To minimize the effect of horizontal transport of air above the canopy on the linkage between the filter-based data and the optical parameters, we selected the data that showed significant vertical transport of aerosols from the forest canopy to the air above. Significant vertical transport was defined by the local horizontal and vertical wind speeds measured at the forest canopy crane with a vertical height of 25 m at the forest site. Specifically, the data with the horizontal wind speeds < 3.5 m s^{-1} were selected first which are assumed to be less influenced by horizontal transport. Then the data with the positive vertical winds (i.e., from the canopy to the above atmosphere) were further selected to be defined as the significant vertical transport.

3. Results and Discussion

3.1. Seasonal trends of the aerosol chemical composition and AOD

Fig. 2a presents the temporal variations of the WSA mass concentration and the daily averaged AOD at a wavelength of 500 nm from June to December 2015. The mass concentrations of WSA ranged from 0.31 to 10.65 μg m^{-3} with an average of 4.46 ± 2.31 μg m^{-3}. Significant increases in the concentrations of the WSA were observed in three periods:

July 20-August 22, October 17-November 5, and September 21-October 1 which are referred to as summer, autumn, and transition period, respectively. The AOD ranged from 0.03 to 0.72 with an average of 0.18 ± 0.13. This average value is similar to that reported by Eck et al. (2009), who showed that monthly averaged AOD at the wavelength of 500 nm was less than 0.10 at a boreal background site in Central Alaska. As stated in section 2.3, an increase in AOD (>0.4) observed in summer indicates high aerosol loadings in this season. Indeed, the concentrations of WSA and the AOD show a significant positive correlation (R^2 = 0.76). Although the number of the WSA samples is limited (n = 15), the positive correlation suggests a close linkage between the two parameters.

Fig. 2b shows the seasonal variation in the mass concentrations of WSOM and sulfate, whereas **Fig. 2c** presents the chemical mass fractions in WSA. During the first half of summer, ~60% of the WSA mass was sulfate (up to 3.40 μg m^{-3}). In contrast, WSOM accounted for ~70% of the WSA mass in autumn, the concentration reaching as large as 7.50 μg m^{-3}. Müller et al. (2017) reported similar temporal trends of the fractions and concentrations for WSOM, and sulfate for the data in 2013 at the same forest site. They made positive matrix factorization (PMF) for the source apportionment of the observed aerosols by using various molecular tracers of biogenic sources as well as anthropogenic sources. The PMF analysis distinguished the contributions of biogenic and anthropogenic sources to the observed aerosols. Müller et al. (2017) indicated that the increased concentrations and fractions of sulfate in summer were attributable to the inflow of anthropogenic aerosols from the urban area, whereas those of WSOM in autumn were mostly attributed to BSOA from the forest floor.

To examine the dominant sources of the observed aerosols for each season in this study, **Fig. 2d** shows the local wind direction and wind speeds at the forest site. In summer, southerly winds were predominant, indicating that the observed aerosols were mainly

transported from the coastal industrial area of Tomakomai city (**Fig. 1**). Moreover, the contribution of sea-salt sulfate to the total sulfate mass was negligible (< 2%). These result suggests that the increased concentration of sulfate in summer was attributable to the anthropogenic sources, the result of which is similar to that obtained in 2013 (Müller et al., 2017). On the other hand, northerly wind was predominant in autumn (**Fig. 2d**), indicating that the observed increase in the WSOM concentrations was mainly associated with the influence from the forest area in this season (**Fig. 1**). This result is also similar to that obtained by Müller et al. (2017). In summary, the overall result suggests that anthropogenic sulfate and biogenic WSOM dominated the WSA in the forest canopy in summer and autumn, respectively.

3.2. Ångström exponent, AOD, and water-soluble aerosols (WSA)

Fig. 2e shows the seasonal variation of the daily averaged AE. The average AE value was 1.19 ± 0.28, most of which exceeded 1.00 during the study period (**Table 1**). As described in section 2.3, the AE with mostly >1.00 indicates the dominance of submicrometer aerosols. The result suggests that the variation in AOD was associated with the chemical composition of submicrometer aerosols. In previous studies, the dependence of satellite-derived AOD on the characteristics of aerosol particles were reported in central and suburban Helsinki and over the United States, including the coastal regions (Natunen et al., 2010; Toth et al., 2014). Using ground- and satellite-based AOD retrievals at urban and suburban sites in Singapore, Chew et al. (2016) found a significant positive correlation between AOD and $PM_{2.5}$ (particulate matter with a diameter less than 2.5 μm), when the aerosol layer existed near the surface or the planetary boundary layer (PBL) was well-mixed.

In addition, other previous studies showed that AOD can be affected by emissions of BVOCs and chemical compositions of WSA (Goldstein et al., 2009; Mielonen et al., 2018; Nguyen et al., 2016). Nguyen et al. (2016) attributed the increase in AOD to the increase of hygroscopic sulfate particles over the southeast United States during summer. Goldstein et al. (2009) and Mielonen et al. (2018) found a relation between increased AOD and increased emissions of BVOC from forests in southeastern USA. In our study, the local wind data indicates the significance of vertical transport of air masses, indicating that the AOD during the study period was largely influenced by the increased mass concentrations of submicrometer WSA in the forest canopy.

3.3. Impact of the biogenic emissions of organic matter on light-scattering and absorbing characteristics of aerosols

To investigate the influence of biogenic emissions of organic matter on light-scattering and light-absorbing characteristics of aerosols above the forest canopy, **Fig. 2f** shows the temporal variation of the daily averaged SSA at a wavelength of 500 nm. In summer, the average SSA was 0.98 ± 0.01, most of which were larger than 0.95, indicating that the observed aerosols had mainly scattering characteristics. In contrast, most of the SSA in autumn ranged 0.90–0.95 (with an average of 0.93 ± 0.02); this was generally lower than the SSA in summer (an average of 0.98 ± 0.01) and the transition period (an average of 0.95 ± 0.02) by 5% and 2%, respectively (**Table 1**). The difference in the SSA in each season suggests that the aerosols above the forest canopy in autumn have more light-absorbing characteristics.

It has been demonstrated that some types of organic carbon (OC) in aerosols show strong light absorption at visible and UV wavelengths (e.g., Bahadur et al., 2012; Giles et al.,

2012; Moise et al., 2015). Müller et al. (2017) suggested that the increase in the WSOM mass in autumn was attributable to the emissions of α-pinene from the forest floor and the subsequent formation of SOA. Light-absorbing characteristics of α-pinene SOA have been reported by laboratory experiments (Lambe et al., 2013; Song et al., 2013; Zhong and Jang, 2011). Song et al. (2013) found significant light absorption at 355 nm and 405 nm by SOA formed from ozonolysis and NO_3 oxidation of α-pinene in the presence of highly acidic sulfate seed aerosols under dry conditions. Our results in the current study imply that biogenic emissions of organic matter from the forest floor and subsequent formation of SOA might increase the absorption characteristics of the particles in autumn.

Fig. 3 shows the dependence of SSA on wavelength during the summer and autumn periods for the data of AOD larger than 0.2. The data with AOD < 0.2 was excluded for the following analysis to focus on possible sources of aerosols with these high AOD. Generally, no spectral dependence of SSA was observed during summer (**Fig. 3a**). In contrast, the SSA in autumn showed a strong dependence on wavelength, which were lower at shorter wavelength (<600 nm) in that season (**Fig. 3b**). Previous studies found that hygroscopic aerosol particles such as sulfate have near neutral spectral dependence on SSA (e.g., Giles et al., 2012); however, the SSA of BC, urban-industrial aerosols, and biomass burning aerosols decreased as the wavelength increased (e.g., Dubovik et al., 2002; Giles et al., 2012; Li et al., 2015; Russell et al., 2010). Yet the SSA of aerosol particles dominated by OC have been characterized as increasing with increases in wavelength (Bahadur et al., 2012; Cazorla et al., 2013; Giles et al., 2012; Russell et al., 2010), which has been explained by the strong light absorption in the wavelength range between 350 nm 470 nm. Indeed, many types of organic species show light-absorbing characteristics at this wavelength range (e.g., Andreae and Gelencsér, 2006; Kirchstetter et al., 2004; Lambe et al., 2013; Song et al., 2013; Yang et al., 2009). Russell et al. (2010) showed that for urban aerosols in Mexico City, the spectral

311 dependence of SSA on wavelength changed from negative to positive with increasing
312 fractions of organic mass in aerosol particles. In this study, the difference in the spectral
313 dependence on the wavelength between summer and autumn suggests that hygroscopic
314 aerosol particles contributed to less light-absorbing characteristics in summer, whereas
315 particles dominated by organic matter contributed to more light-absorbing characteristics in
316 autumn. This is supported by the dominant chemical component in summer (sulfate) and
317 autumn (WSOM) as discussed above (**Fig. 2b** and **Fig. 2c**).

318 **Fig. 4** shows a scatterplot of AAE and SAE, for the data of AOD >0.2 in summer and
319 autumn. In autumn, the AAE and SAE showed relatively larger values with averages of 2.45
320 ± 0.91 and 1.46 ± 0.15, respectively. On the other hand, in summer, the majority (85%) of the
321 data have relatively smaller values less than 2.5 and 1.5 for AAE and SAE, respectively. The
322 result indicates that small particles with strong light absorption at shorter wavelength were
323 dominant in autumn, whereas larger particles with less light-absorbing properties were more
324 evident in summer. Previous studies showed that light-absorbing OC aerosols in smaller size
325 ranges are indicated by AAE > 1.5 and SAE > 1.5. Using ground-based remote sensing
326 techniques, Russell et al. (2010) found that the increased mass fraction of organic matter in
327 submicrometer aerosols corresponded to an AAE of 1.5 in boreal forests in the USA and
328 Canada. Bahadur et al. (2012) investigated the AAE of OC aerosols at various urban
329 industrial and background sites and reported the global average to be 4.55 ± 2.01. Therefore,
330 the higher AAE values in autumn from this study imply a significant influence of OC on
331 light-absorbing properties; this is consistent with the results of previous works.

332 In summary, the current study indicates that biogenic organic aerosols observed in the
333 forest canopy can affect the optical properties of aerosol above the canopy. Namely, the lower
334 SSA in autumn indicates that the light absorption by smaller aerosol particles was more
335 significant than in summer. As stated above, our previous study indicated that the observed

WSOM, which was a dominant component in autumn, was associated with emission of organic matter from the forest floor (Müller et al., 2017). Therefore, the subsequent formation of BSOA is closely linked with the enhanced light-absorbing properties of the aerosol particles in this season. This might have important implications for the prediction of the radiative effect of biogenic organic aerosols produced in forest area on a regional scale in future.

Conclusions

The current study indicates that biogenic secondary organic aerosols (BSOAs) observed in the canopy of a cool-temperate forest can affect the optical properties of aerosol above the canopy. Namely, the lower SSA in autumn indicates that the light absorption by smaller aerosol particles was more significant than in summer. As stated above, our previous study indicated that the observed WSOM, which was a dominant component in autumn, was associated with emission of organic matter (mostly α-pinene) from the forest floor (Müller et al., 2017). Therefore, the subsequent formation of BSOAs is closely linked with the enhanced light-absorbing properties of the aerosol particles in this season.

The study suggests the importance of BSOA from the forest for the impact on the scattering/absorption characteristics of aerosols above the forest canopy. This impact should be considered for the prediction of the aerosol radiative forcing on a regional scale and the effect of biogenic organic aerosols on climate in future. Additional field studies at other forest sites and comprehensive in-situ and remote sensing measurements are required to confirm the results and to elucidate the detailed mechanism of how BSOA affect the optical properties on regional and global scale.

Acknowledgments. This research was supported in part by JSPS KAKENHI (grant numbers 16H02931 and 25281002) by the Ministry of Education, Culture, Sports, Science and Technology (MEXT) of Japan. This work was also supported by the JAXA GCOM-C science project. All data used in this study is provided in the supporting information.

References

Andreae, M.O., Gelencsér, A., 2006. Black carbon or brown carbon? The nature of light-absorbing carbonaceous aerosols. Atmos. Chem. Phys. 6, 3131–3148. https://doi.org/10.5194/acp-6-3131-2006

Andrews, E., Ogren, J.A., Kinne, S., Samset, B., 2017. Comparison of AOD, AAOD and column single scattering albedo from AERONET retrievals and in situ profiling measurements. Atmos. Chem. Phys. 17, 6041–6072. https://doi.org/10.5194/acp-17-6041-2017

Ångström, A., 1964. The parameters of atmospheric turbidity. Tellus 16, 64–75. https://doi.org/10.1111/j.2153-3490.1964.tb00144.x

Aoki, K., Nakajima, T., Takamura, T., 2008. Aerosol and cloud optical properties by ground-based sky radiometer measurements, Proceedings of SPIE. p. 70270U. https://doi.org/10.1117/12.822504

Aoki, K., Fujiyoshi, Y., 2003. Sky Radiometer Measurements of Aerosol Optical Properties over Sapporo, Japan. J. Meteorol. Soc. Japan 81, 493–513. https://doi.org/10.2151/jmsj.81.493

Aoki, K., Takemura, T., Kawamoto, K., Hayasaka, T., 2013. Aerosol climatology over Japan site measured by ground-based sky radiometer. AIP Conf. Proc. pp. 284–287. https://doi.org/10.1063/1.4804762

Bahadur, R., Praveen, P.S., Xu, Y., Ramanathan, V., 2012. Solar absorption by elemental and brown carbon determined from spectral observations. Proc. Natl. Acad. Sci. 109, 17366–17371. https://doi.org/10.1073/pnas.1205910109

Balkanski, Y., Schulz, M., Claquin, T., Guibert, S., 2007. Reevaluation of Mineral aerosol radiative forcings suggests a better agreement with satellite and AERONET data. Atmos. Chem. Phys. 7, 81–95. https://doi.org/10.5194/acp-7-81-2007

Bergstrom, R.W., Pilewskie, P., Russell, P.B., Redemann, J., Bond, T.C., Quinn, P.K., Sierau, B., 2007. Spectral absorption properties of atmospheric aerosols. Atmos. Chem. Phys. 7, 5937–5943. https://doi.org/10.5194/acp-7-5937-2007

Cappa, C.D., Kolesar, K.R., Zhang, X., Atkinson, D.B., Pekour, M.S., Zaveri, R.A., Zelenyuk, A., Zhang, Q., 2016. Understanding the optical properties of ambient sub- and supermicron particulate matter: results from the CARES 2010 field study in northern California. Atmos. Chem. Phys. 16, 6511–6535. https://doi.org/10.5194/acp-16-6511-2016

399 Cazorla, A., Bahadur, R., Suski, K.J., Cahill, J.F., Chand, D., Schmid, B., Ramanathan, V.,
400 Prather, K.A., 2013. Relating aerosol absorption due to soot, organic carbon, and dust to
401 emission sources determined from in-situ chemical measurements. Atmos. Chem. Phys.
402 13, 9337–9350. https://doi.org/10.5194/acp-13-9337-2013
403 Chen, C., Dubovik, O., Henze, D.K., Lapyonak, T., Chin, M., Ducos, F., Litvinov, P., Huang,
404 X., Li, L., 2018. Retrieval of desert dust and carbonaceous aerosol emissions over Africa
405 from POLDER/PARASOL products generated by the GRASP algorithm. Atmos. Chem.
406 Phys. 18, 12551–12580. https://doi.org/10.5194/acp-18-12551-2018
407 Chew, B.N., Campbell, J.R., Hyer, E.J., Salinas, S. V., Reid, J.S., Welton, E.J., Holben, B.N.,
408 Liew, S.C., 2016. Relationship between aerosol optical depth and particulate matter over
409 Singapore: Effects of aerosol vertical distributions. Aerosol Air Qual. Res. 16, 2818–
410 2830. https://doi.org/10.4209/aaqr.2015.07.0457
411 Dubovik, O., Holben, B., Eck, T.F., Smirnov, A., Kaufman, Y.J., King, M.D., Tanré, D.,
412 Slutsker, I., 2002. Variability of Absorption and Optical Properties of Key Aerosol Types
413 Observed in Worldwide Locations. J. Atmos. Sci. 59, 590–608.
414 https://doi.org/10.1175/1520-0469(2002)059<0590:VOAAOP>2.0.CO;2
415 Eck, T.F., Holben, B.N., Reid, J.S., Sinyuk, A., Hyer, E.J., O'Neill, N.T., Shaw, G.E., Vande
416 Castle, J.R., Chapin, F.S., Dubovik, O., Smirnov, A., Vermote, E., Schafer, J.S., Giles,
417 D., Slutsker, I., Sorokine, M., Newcomb, W.W., 2009. Optical properties of boreal
418 region biomass burning aerosols in central Alaska and seasonal variation of aerosol
419 optical depth at an Arctic coastal site. J. Geophys. Res. 114, D11201.
420 https://doi.org/10.1029/2008JD010870
421 FAO, 2001. Global Forest Resources Assessment 2000 Main Report, FAO Forestry Paper
422 140. Rome.
423 Finessi, E., Decesari, S., Paglione, M., Giulianelli, L., Carbone, C., Gilardoni, S., Fuzzi, S.,
424 Saarikoski, S., Raatikainen, T., Hillamo, R., Allan, J., Mentel, T.F., Tiitta, P., Laaksonen,
425 A., Petäjä, T., Kulmala, M., Worsnop, D.R., Facchini, M.C., 2012. Determination of the
426 biogenic secondary organic aerosol fraction in the boreal forest by NMR spectroscopy.
427 Atmos. Chem. Phys. 12, 941–959. https://doi.org/10.5194/acp-12-941-2012
428 Flores, J.M., Washenfelder, R.A., Adler, G., Lee, H.J., Segev, L., Laskin, J., Laskin, A.,
429 Nizkorodov, S.A., Brown, S.S., Rudich, Y., 2014. Complex refractive indices in the
430 near-ultraviolet spectral region of biogenic secondary organic aerosol aged with
431 ammonia. Phys. Chem. Chem. Phys. 16, 10629–10642.
432 https://doi.org/10.1039/C4CP01009D

433 Giles, D.M., Holben, B.N., Eck, T.F., Sinyuk, A., Smirnov, A., Slutsker, I., Dickerson, R.R.,
434 Thompson, a. M., Schafer, J.S., 2012. An analysis of AERONET aerosol absorption
435 properties and classifications representative of aerosol source regions. J. Geophys. Res.
436 Atmos. 117. https://doi.org/10.1029/2012JD018127
437 Goldstein, A.H., Koven, C.D., Heald, C.L., Fung, I.Y., 2009. Biogenic carbon and
438 anthropogenic pollutants combine to form a cooling haze over the southeastern United
439 States. Proc. Natl. Acad. Sci. 106, 8835–8840. https://doi.org/10.1073/pnas.0904128106
440 Guenther, A., Hewitt, C.N., Erickson, D., Fall, R., Geron, C., Graedel, T., Harley, P., Klinger,
441 L., Lerdau, M., Mckay, W.A., Pierce, T., Scholes, B., Steinbrecher, R., Tallamraju, R.,
442 Taylor, J., Zimmerman, P., 1995. A global model of natural volatile organic compound
443 emissions. J. Geophys. Res. 100, 8873. https://doi.org/10.1029/94JD02950
444 Hansen, J., Sato, M., Ruedy, R., 1997. Radiative forcing and climate response. J. Geophys.
445 Res. Atmos. 102, 6831–6864. https://doi.org/10.1029/96JD03436
446 Hiura, T., 2005. Estimation of aboveground biomass and net biomass increment in a cool
447 temperate forest on a landscape scale. Ecol. Res. 20, 271–277.
448 https://doi.org/10.1007/s11284-005-0042-0
449 Jacobson, M.Z., 2001. Strong radiative heating due to the mixing state of black carbon in
450 atmospheric aerosols. Nature 409, 695–697. https://doi.org/10.1038/35055518
451 Kanakidou, M., Seinfeld, J.H., Pandis, S.N., Barnes, I., Dentener, F.J., Facchini, M.C., Van
452 Dingenen, R., Ervens, B., Nenes, A., Nielsen, C.J., Swietlicki, E., Putaud, J.P.,
453 Balkanski, Y., Fuzzi, S., Horth, J., Moortgat, G.K., Winterhalter, R., Myhre, C.E.L.,
454 Tsigaridis, K., Vignati, E., Stephanou, E.G., Wilson, J., 2005. Organic aerosol and global
455 climate modelling: a review. Atmos. Chem. Phys. 5, 1053–1123.
456 https://doi.org/10.5194/acp-5-1053-2005
457 Kim, H., Barkey, B., Paulson, S.E., 2010. Real refractive indices of a - and b - pinene and
458 toluene secondary organic aerosols generated from ozonolysis and photo - oxidation
459 115, 1–10. https://doi.org/10.1029/2010JD014549
460 Kim, H., Paulson, S.E., 2013. Real refractive indices and volatility of secondary organic
461 aerosol generated from photooxidation and ozonolysis of limonene, α-pinene and
462 toluene. Atmos. Chem. Phys. 13, 7711–7723. https://doi.org/10.5194/acp-13-7711-2013
463 Kirchstetter, T.W., Novakov, T., Hobbs, P. V., 2004. Evidence that the spectral dependence of
464 light absorption by aerosols is affected by organic carbon. J. Geophys. Res. Atmos. 109.
465 https://doi.org/10.1029/2004JD004999
466 Koch, D., Bond, T.C., Streets, D., Unger, N., van der Werf, G.R., 2007. Global impacts of

aerosols from particular source regions and sectors. J. Geophys. Res. 112, D02205. https://doi.org/10.1029/2005JD007024

Lack, D.A., Cappa, C.D., 2010. Impact of brown and clear carbon on light absorption enhancement, single scatter albedo and absorption wavelength dependence of black carbon. Atmos. Chem. Phys. 10, 4207–4220. https://doi.org/10.5194/acp-10-4207-2010

Lambe, A.T., Cappa, C.D., Massoli, P., Onasch, T.B., Forestieri, S.D., Martin, A.T., Cummings, M.J., Croasdale, D.R., Brune, W.H., Worsnop, D.R., Davidovits, P., 2013. Relationship between oxidation level and optical properties of secondary organic aerosol. Environ. Sci. Technol. 47, 6349–6357. https://doi.org/10.1021/es401043j

Lee, J., Kim, J., Song, C.H., Kim, S.B., Chun, Y., Sohn, B.J., Holben, B.N., 2010. Characteristics of aerosol types from AERONET sunphotometer measurements. Atmos. Environ. 44, 3110–3117. https://doi.org/10.1016/j.atmosenv.2010.05.035

Levy, R.C., Remer, L.A., Dubovik, O., 2007. Global aerosol optical properties and application to Moderate Resolution Imaging Spectroradiometer aerosol retrieval over land. J. Geophys. Res. Atmos. 112, 1–15. https://doi.org/10.1029/2006JD007815

Li, J., Carlson, B.E., Lacis, A.A., 2015. Using single-scattering albedo spectral curvature to characterize East Asian aerosol mixtures. J. Geophys. Res. Atmos. 120, 2037–2052. https://doi.org/10.1002/2014JD022433

Lihavainen, H., Kerminen, V.-M., Tunved, P., Aaltonen, V., Arola, A., Hatakka, J., Hyvärinen, A., Viisanen, Y., 2009. Observational signature of the direct radiative effect by natural boreal forest aerosols and its relation to the corresponding first indirect effect. J. Geophys. Res. 114, D20206. https://doi.org/10.1029/2009JD012078

Mielonen, T., Hienola, A., Kühn, T., Merikanto, J., Lipponen, A., Bergman, T., Korhonen, H., Kolmonen, P., Sogacheva, L., Ghent, D., Pitkänen, M.R.A., Arola, A., de Leeuw, G., Kokkola, H., 2018. Summertime aerosol radiative effects and their dependence on temperature over the southeastern USA. Atmosphere (Basel). 9, 1–23. https://doi.org/10.3390/atmos9050180

Miyazaki, Y., Aggarwal, S.G., Singh, K., Gupta, P.K., Kawamura, K., 2009. Dicarboxylic acids and water-soluble organic carbon in aerosols in New Delhi, India, in winter: Characteristics and formation processes. J. Geophys. Res. 114, D19206. https://doi.org/10.1029/2009JD011790

Miyazaki, Y., Fu, P., Ono, K., Tachibana, E., Kawamura, K., 2014. Seasonal cycles of water-soluble organic nitrogen aerosols in a deciduous broadleaf forest in northern Japan. J. Geophys. Res. Atmos. 119, 1440–1454. https://doi.org/10.1002/2013JD020713

Miyazaki, Y., Jung, J., Fu, P., Mizoguchi, Y., Yamanoi, K., Kawamura, K., 2012. Evidence of formation of submicrometer water-soluble organic aerosols at a deciduous forest site in northern Japan in summer. J. Geophys. Res. Atmos. 117. https://doi.org/10.1029/2012JD018250

Moise, T., Flores, J. M., Rudich, Y., 2015. Optical Properties of Secondary Organic Aerosols and Their Changes by Chemical Processes. Chem. Rev. 115, 4400–4439. https://doi.org/10.1021/cr5005259

Müller, A., Miyazaki, Y., Tachibana, E., Kawamura, K., Hiura, T., 2017. Evidence of a reduction in cloud condensation nuclei activity of water-soluble aerosols caused by biogenic emissions in a cool-temperate forest. Sci. Rep. 7, 8452. https://doi.org/10.1038/s41598-017-08112-9

Myhre, G., Shindell, D., Bréon, F.-M., Collins, W., Fuglestvedt, J., Huang, J., Koch, D., Lamarque, J.-F., Lee, D., Mendoza, B., Nakajima, T., Robock, A., Stephens, G., Takemura, T., Zhang, H., 2013. Anthropogenic and Natural Radiative Forcing, in: Climate Change 2013: The Physical Science Basis. Contribution of Working Group I to the Fifth Assessment Report of the Intergovernmental Panel on Climate Change. pp. 659–740. https://doi.org/10.1017/CBO9781107415324.018

Nakajima, T., Tonna, G., Rao, R., Boi, P., Kaufman, Y., Holben, B., 1996. Use of sky brightness measurements from ground for remote sensing of particulate polydispersions. Appl. Opt. 35, 2672. https://doi.org/10.1364/AO.35.002672

Nakayama, T., Matsumi, Y., Sato, K., Imamura, T., Yamazaki, A., Uchiyama, A., 2010. Laboratory studies on optical properties of secondary organic aerosols generated during the photooxidation of toluene and the ozonolysis of α-pinene. J. Geophys. Res. Atmos. 115, 1–11. https://doi.org/10.1029/2010JD014387

Natunen, A., Arola, A., Mielonen, T., Huttunen, J., Komppula, M., Lehtinen, K.E.J., 2010. A multi-year comparison of PM2.5 and AOD for the helsinki region. Boreal Environ. Res. 15, 544–552.

Nguyen, T.K. V, Ghate, V.P., Carlton, A.G., 2016. Reconciling satellite aerosol optical thickness and surface fine particle mass through aerosol liquid water. Geophys. Res. Lett. 1–10. https://doi.org/10.1002/2016GL070994

Ramanathan, V., Carmichael, G., 2008. Global and Regional Climate Changes Due to Black Carbon. Nat. Geosci., 1, 221–227. https://doi.org/10.1038/ngeo156

Rinne, J., Bäck, J., Hakola, H., 2009. Biogenic volatile organic compound emissions from the Eurasian taiga: Current knowledge and future directions. Boreal Environ. Res. 14, 807–

826.

Russell, P.B., Bergstrom, R.W., Shinozuka, Y., Clarke, A.D., DeCarlo, P.F., Jimenez, J.L., Livingston, J.M., Redemann, J., Dubovik, O., Strawa, A., 2010. Absorption Angstrom Exponent in AERONET and related data as an indicator of aerosol composition. Atmos. Chem. Phys. 10, 1155–1169. https://doi.org/10.5194/acp-10-1155-2010

Salinas, S. V., Chew, B.N., Miettinen, J., Campbell, J.R., Welton, E.J., Reid, J.S., Yu, L.E., Liew, S.C., 2013. Physical and optical characteristics of the October 2010 haze event over Singapore: A photometric and lidar analysis. Atmos. Res. 122, 555–570. https://doi.org/10.1016/j.atmosres.2012.05.021

Salinas, S. V, Chew, B.N., Liew, S.C., 2009. Retrievals of aerosol optical depth and Angström exponent from ground-based Sun-photometer data of Singapore. Appl. Opt. 48, 1473–84.

Schmeisser, L., Andrews, E., Ogren, J.A., Sheridan, P., Jefferson, A., Sharma, S., Kim, J.E., Sherman, J.P., Sorribas, M., Kalapov, I., Arsov, T., Angelov, C., Mayol-Bracero, O.L., Labuschagne, C., Kim, S.-W., Hoffer, A., Lin, N.-H., Chia, H.-P., Bergin, M., Sun, J., Liu, P., Wu, H., 2017. Classifying aerosol type using in situ surface spectral aerosol optical properties. Atmos. Chem. Phys. 17, 12097–12120. https://doi.org/10.5194/acp-17-12097-2017

Schuster, G.L., Dubovik, O., Holben, B.N., 2006. Angstrom exponent and bimodal aerosol size distributions. J. Geophys. Res. Atmos. 111, 1–14. https://doi.org/10.1029/2005JD006328

Scott, C.E., Rap, a., Spracklen, D. V., Forster, P.M., Carslaw, K.S., Mann, G.W., Pringle, K.J., Kivekäs, N., Kulmala, M., Lihavainen, H., Tunved, P., 2014. The direct and indirect radiative effects of biogenic secondary organic aerosol. Atmos. Chem. Phys. 14, 447–470. https://doi.org/10.5194/acp-14-447-2014

Shibata, H., Kirikae, M., Tanaka, Y., Sakuma, T., Hatano, R., 1998. Proton Budgets of Forest Ecosystems on Volcanogenous Regosols in Hokkaido, Northern Japan. Water. Air. Soil Pollut. 105, 63–72. https://doi.org/10.1023/A:1005086400473

Song, C., Gyawali, M., Zaveri, R.A., Shilling, J.E., Arnott, W.P., 2013. Light absorption by secondary organic aerosol from α-pinene: Effects of oxidants, seed aerosol acidity, and relative humidity. J. Geophys. Res. Atmos. 118, 11741–11749. https://doi.org/10.1002/jgrd.50767

Takafumi, H., Hiura, T., 2009. Effects of disturbance history and environmental factors on the diversity and productivity of understory vegetation in a cool-temperate forest in Japan.

For. Ecol. Manage. 257, 843–857. https://doi.org/10.1016/j.foreco.2008.10.020

Toth, T.D., Zhang, J., Campbell, J.R., Hyer, E.J., Reid, J.S., Shi, Y., Westphal, D.L., 2014. Impact of data quality and surface-to-column representativeness on the PM2.5 / satellite AOD relationship for the contiguous United States. Atmos. Chem. Phys. 14, 6049–6062. https://doi.org/10.5194/acp-14-6049-2014

Wang, X., Heald, C.L., Ridley, D.A., Schwarz, J.P., Spackman, J.R., Perring, A.E., Coe, H., Liu, D., Clarke, A.D., 2014. Exploiting simultaneous observational constraints on mass and absorption to estimate the global direct radiative forcing of black carbon and brown carbon. Atmos. Chem. Phys. 14, 10989–11010. https://doi.org/10.5194/acp-14-10989-2014

Yang, M., Howell, S.G., Zhuang, J., Huebert, B.J., 2009. Attribution of aerosol light absorption to black carbon, brown carbon, and dust in China – interpretations of atmospheric measurements during EAST-AIRE. Atmos. Chem. Phys. 9, 2035–2050. https://doi.org/10.5194/acp-9-2035-2009

Yttri, K.E., Aas, W., Bjerke, A., Cape, J.N., Cavalli, F., Ceburnis, D., Dye, C., Emblico, L., Facchini, M.C., Forster, C., Hanssen, J.E., Hansson, H.C., Jennings, S.G., Maenhaut, W., Putaud, J.P., Tørseth, K., 2007. Elemental and organic carbon in PM10: a one year measurement campaign within the European Monitoring and Evaluation Programme EMEP. Atmos. Chem. Phys. 7, 5711–5725. https://doi.org/10.5194/acp-7-5711-2007

Zhong, M., Jang, M., 2011. Light absorption coefficient measurement of SOA using a UV-Visible spectrometer connected with an integrating sphere. Atmos. Environ. 45, 4263–4271. https://doi.org/10.1016/j.atmosenv.2011.04.082

Table 1. Average or individual values of the optical and chemical parameters for the three periods in 2015: summer (Jul. 20–Aug. 22), a transition period (Sept. 21–Oct. 1), and autumn (Oct. 17–Nov. 5). The number of data points for the optical parameters (ND_{opt}) and the filter-based chemical parameters (ND_{filter}) are shown for each season.

	Summer ND_{opt} =129, ND_{filter} = 2 (Jul. 20—Aug. 22)	**Transition period** ND_{opt} = 30 ND_{filter} = 2 (Sept. 21–Oct. 1)	**Autumn** ND_{opt} = 159 ND_{filter} = 3 (Oct. 17–Nov. 5)
Aerosol optical depth (AOD) at λ = 500 nm	0.31 ± 0.18	0.25 ± 0.06	0.18 ± 0.09
Ångström exponent (AE)	1.29 ± 0.04	1.22 ± 0.04	1.39 ± 0.04
Single scattering albedo (SSA) at λ = 500 nm	0.98 ± 0.01	0.95 ± 0.02	0.93 ± 0.02
Absorption Ångström exponent (AAE)	1.15 ± 0.84	0.78 ± 0.47	2.45 ± 0.91
Scattering Ångström exponent (SAE)	1.25 ± 0.22	1.13 ± 0.06	1.46 ± 0.15
SO_4^{2-} (μg m^{-3})	2.15, 3.40	1.67, 0.43	1.04 ± 0.50
WSOM (μgm^{-3})	0.59, 1.37	0.74, 0.69	4.02 ± 2.51
WSA (μg m^{-3})	3.45, 5.89	2.93, 1.31	5.79 ± 3.50

Figure Captions

Fig. 1. Location of the sampling site: Tomakomai Experimental Forest of Hokkaido university, Hokkaido, northern Japan. Map data ©2018 Google, ZENRIN; Imagery ©2018 Google, DigitalGlobe, Data SIO, NOAA, U.S. Navy, NGA, GEBCO, TerraMetrics (https://maps.google.com/). Maps are modified with Microsoft PowerPoint 2013.

Fig. 2. Time series of (a) the concentration of submicron water-soluble aerosols (WSA) obtained by the filter-based measurements and the aerosol optical depth (AOD) at a wavelength of 500 nm, (b) the mass concentrations of submicrometer water-soluble organic matter (WSOM) and sulfate, (c) the chemical mass fraction of the submicrometer WSA, (d) local wind direction and wind speeds, (e) the Ångström exponent (AE), and (f) the single scattering albedo (SSA) at λ = 500 nm from June to December, 2015. The temporal resolution of the filter-based chemical data is approximately 1 week. For the optical properties, the temporal resolution is one day, where the daily averaged values with the standard deviations are presented. Shaded areas indicate the three periods defined as summer (July 20–August 22), transition period (September 21–October 1), and autumn (October 17–November 5).

Fig. 3. Wavelength dependence of the single scattering albedo (SSA) during (a) the summer period and (b) the autumn period with AOD > 0.2. Gray symbols indicate the daily average values, whereas red symbols show the average values of those daily average SSA.

Fig. 4. Scatter plot of the absorption Ångström exponent (AAE) and the scattering Ångström exponent (SAE) for the summer period (blue) and the autumn period (red) with AOD > 0.2.

Fig. 1

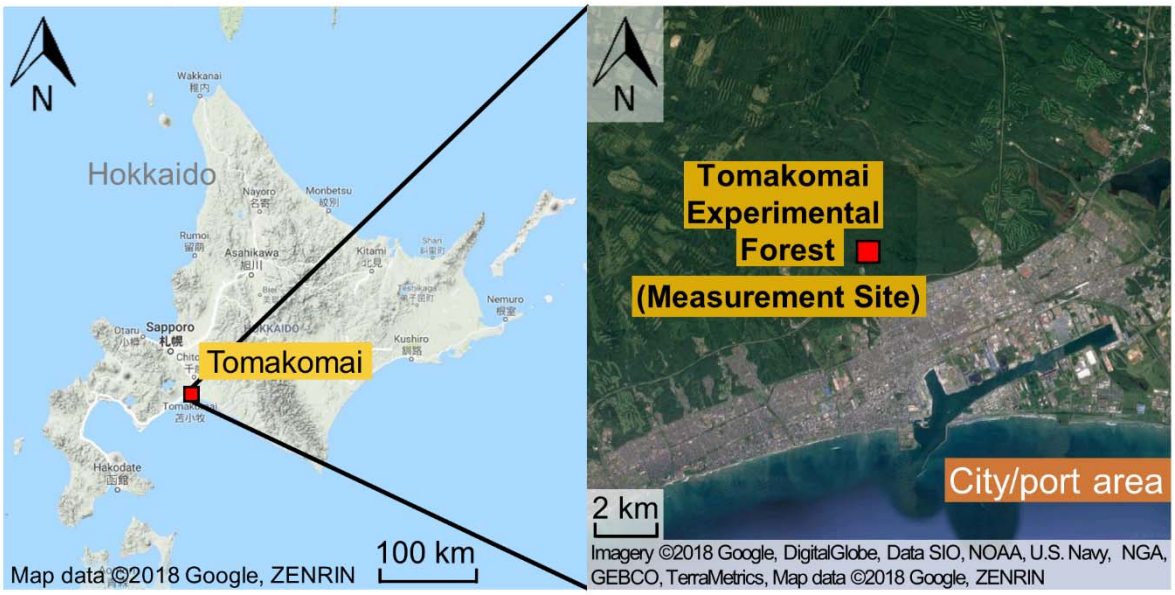
N
Hokkaido
Wakkanai
Nayoro
Monbetsu
Rumoi
Asahikawa
Kitami
Nemuro
Otaru
Sapporo
札幌
Chitose
Tomakomai
苫小牧
Kushiro
Hakodate
函館
100 km
Map data ©2018 Google, ZENRIN
N
Tomakomai
Experimental
Forest
(Measurement Site)
City/port area
2 km
Imagery ©2018 Google, DigitalGlobe, Data SIO, NOAA, U.S. Navy, NGA, GEBCO, TerraMetrics, Map data ©2018 Google, ZENRIN

Fig. 2

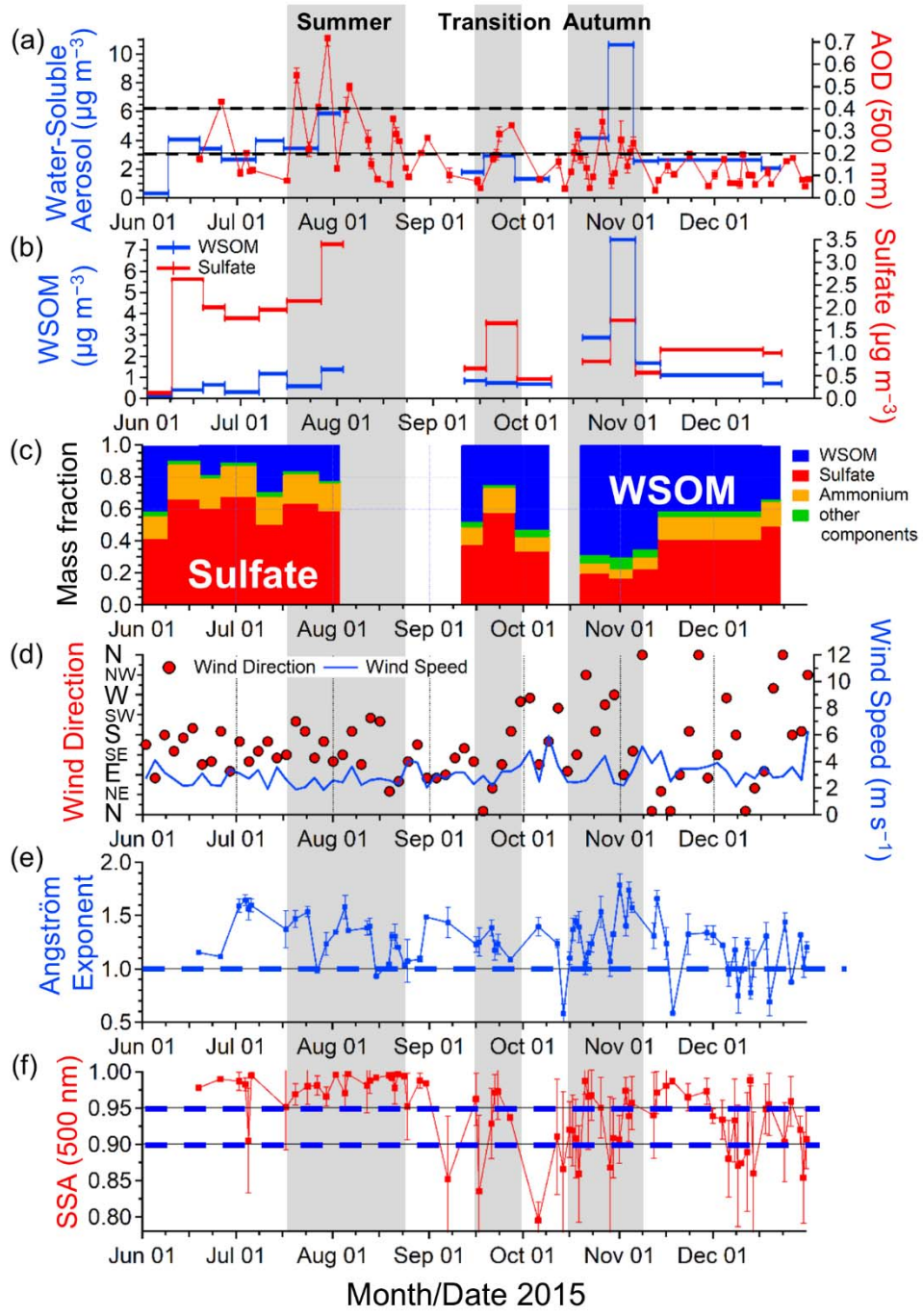
Summer
Transition
Autumn
(a)
Water-Soluble Aerosol (μg m⁻³)
AOD (500 nm)
(b)
WSOM (μg m⁻³)
Sulfate (μg m⁻³)
WSOM
Sulfate
(c)
Mass fraction
Sulfate
WSOM
Ammonium
other components
(d)
Wind Direction
Wind Speed
Wind Speed (m s⁻¹)
(e)
Angström Exponent
(f)
SSA (500 nm)
Jun 01
Jul 01
Aug 01
Sep 01
Oct 01
Nov 01
Dec 01
Month/Date 2015

Fig. 3

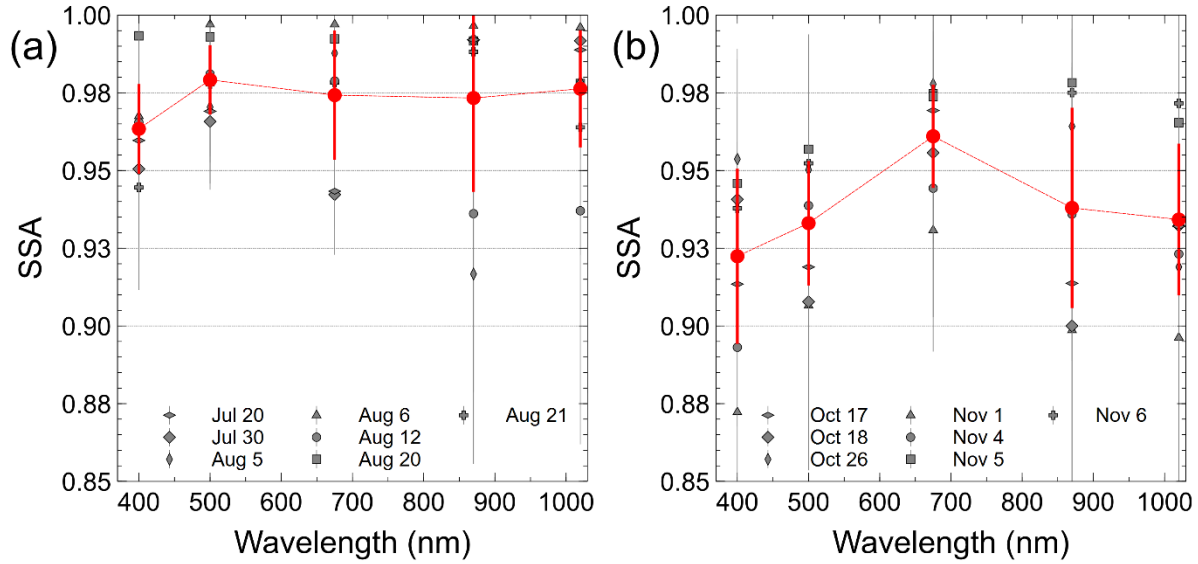
(a)
SSA
Wavelength (nm)
1.00
0.98
0.95
0.93
0.90
0.88
0.85
400
500
600
700
800
900
1000
Jul 20
Jul 30
Aug 5
Aug 6
Aug 12
Aug 20
Aug 21
(b)
SSA
Wavelength (nm)
Oct 17
Oct 18
Oct 26
Nov 1
Nov 4
Nov 5
Nov 6

Fig. 4

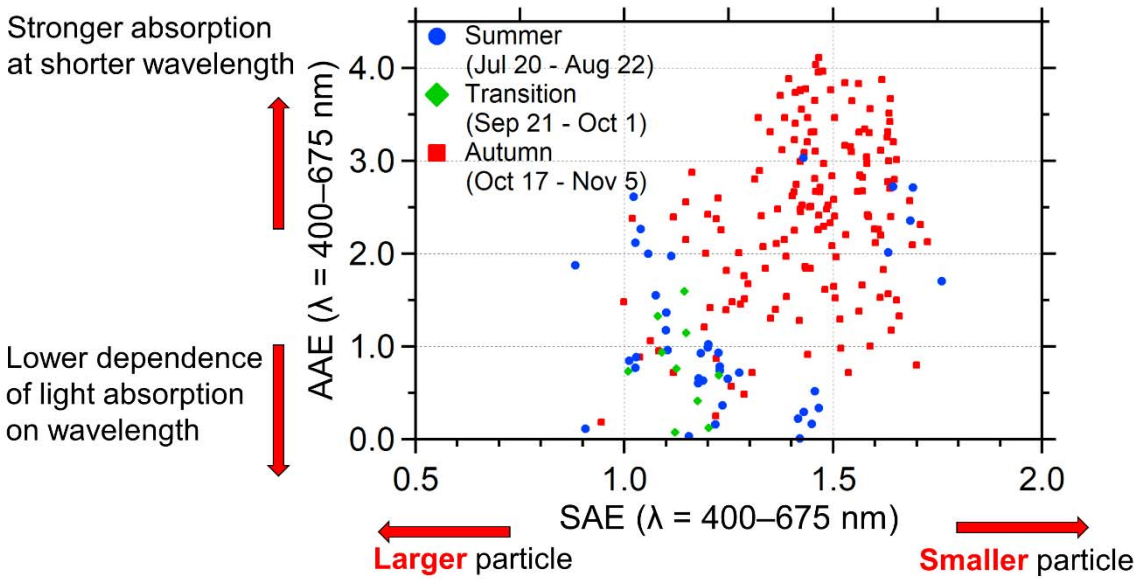
Stronger absorption
at shorter wavelength
Lower dependence
of light absorption
on wavelength
AAE (λ = 400–675 nm)
4.0
3.0
2.0
1.0
0.0
Summer
(Jul 20 - Aug 22)
Transition
(Sep 21 - Oct 1)
Autumn
(Oct 17 - Nov 5)
0.5
1.0
1.5
2.0
SAE (λ = 400–675 nm)
Larger particle
Smaller particle

Appendix A. Supplementary Data:

Impact of biogenic emissions of organic matter from a cool-temperate forest on aerosol optical properties retrieved from a Sky Radiometer

Astrid Müller[a, 1], Kazuma Aoki[b], Eri Tachibana[a], Tsutom Hiura[c], and Yuzo Miyazaki[a, *]

a *Institute of Low Temperature Science, Hokkaido University, Sapporo 060-0819, Japan*
b *Graduate School of Science and Engineering, University of Toyama, Toyama, 930-8555, Japan*
c *Field Science Center for Northern Biosphere, Hokkaido University, Sapporo 060-0809, Japan*

* Corresponding Author
Email address: yuzom@lowtem.hokudai.ac.jp (Y. Miyazaki)

[1] Present address: *Center for Global Environmental Research, National Institute for Environmental Studies, 16-2 Onogawa, Tsukuba, Ibaraki 305-8506, Japan*.

Table S1. The mass concentrations of water-soluble aerosols (WSA), sulfate, and water-soluble organic matter (WSOM) during each sampling period in 2015.

Sampling start date (MM/DD)	Sampling end date (MM/DD)	WSA (μg m^{-3})	Sulfate (μg m^{-3})	WSOM (μg m^{-3})
05/28	06/09	0.313	0.13	0.130
06/09	06/19	4.056	2.64	0.414
06/19	06/26	3.410	2.01	0.658
06/26	07/07	2.676	1.77	0.304
07/07	07/16	3.969	1.96	1.170
07/16	07/27	3.451	2.15	0.591
07/27	08/03	5.888	3.40	1.373
09/11	09/18	1.803	0.66	0.849
09/18	09/28	2.930	1.67	0.742
09/28	10/09	1.313	0.43	0.686
10/19	10/28	4.157	0.82	2.878
10/28	11/05	10.647	1.73	7.496
11/05	11/13	2.562	0.57	1.685
11/13	12/16	2.650	1.08	1.116
12/16	12/22	2.059	1.01	0.715

Table S2. The daily average (Avg.) values with the standard deviation (Std.) of the Aerosol optical depth (AOD) at a wavelength of 500 nm, Ångström exponent (AE), and single scattering albedo (SSA) at 500 nm during the study period from June 19 to December 31, 2015.

	AOD (λ = 500 nm)		**AE**		**SSA (λ = 500 nm)**	
Date (MM/DD)	**Avg.**	**Std.**	**Avg.**	**Std.**	**Avg.**	**Std.**
06/19	0.17	0.00	1.15	0.00	0.98	0.00
06/26	0.43	0.00	1.12	0.00	0.99	0.00
07/02	0.11	0.01	1.59	0.06	0.99	0.01
07/04	0.20	0.01	1.64	0.05	0.98	0.01
07/05	0.12	0.01	1.56	0.10	0.91	0.07
07/06	0.12	0.01	1.60	0.06	1.00	0.00
07/17	0.08	0.01	1.37	0.18	0.95	0.06
07/20	0.55	0.03	1.47	0.08	0.97	0.01
07/24	0.22	0.03	1.54	0.05	0.98	0.02
07/27	0.41	0.01	0.98	0.02	0.98	0.01
07/30	0.72	0.04	1.23	0.11	0.97	0.01
08/02	0.13	0.00	1.35	0.00	1.00	0.00
08/05	0.39	0.06	1.58	0.11	0.97	0.02
08/06	0.50	0.02	1.36	0.00	1.00	0.00
08/12	0.26	0.04	1.38	0.07	0.98	0.04
08/13	0.15	0.02	1.40	0.08	0.99	0.02
08/15	0.08	0.00	0.93	0.00	0.99	0.00
08/19	0.06	0.00	1.05	0.00	1.00	0.00
08/20	0.36	0.00	1.30	0.03	0.99	0.01
08/21	0.29	0.03	1.31	0.11	0.98	0.02
08/22	0.26	0.01	1.20	0.00	1.00	0.00
08/24	0.13	0.01	1.03	0.03	0.99	0.00
08/25	0.09	0.01	1.07	0.20	0.95	0.05
08/29	0.20	0.01	1.09	0.03	0.99	0.01
08/31	0.27	0.00	1.49	0.00	0.98	0.00
09/07	0.10	0.03	1.44	0.14	0.85	0.09
09/16	0.07	0.02	1.23	0.07	0.96	0.04
09/17	0.04	0.00	1.25	0.13	0.84	0.10
09/21	0.18	0.02	1.38	0.07	0.93	0.05
09/22	0.19	0.02	1.17	0.09	0.97	0.03
09/23	0.29	0.03	1.23	0.09	0.97	0.04
09/27	0.33	0.00	1.09	0.00	0.94	0.00
10/06	0.08	0.01	1.39	0.09	0.80	0.02
10/12	0.16	0.03	1.24	0.04	0.91	0.08
10/14	0.04	0.00	0.58	0.09	0.87	0.11
10/16	0.12	0.01	1.10	0.06	0.92	0.04
10/17	0.20	0.04	1.37	0.10	0.92	0.05
10/18	0.28	0.03	1.44	0.05	0.91	0.05

10/19	0.18	0.03	1.39	0.15	0.86	0.07
10/21	0.13	0.05	1.05	0.10	0.99	0.02
10/22	0.04	0.01	1.15	0.10	0.97	0.07
10/23	0.09	0.01	1.24	0.08	0.97	0.03
10/26	0.34	0.05	1.54	0.15	0.95	0.04
10/29	0.08	0.03	1.07	0.14	0.87	0.10
10/30	0.11	0.00	1.33	0.02	0.91	0.05
11/01	0.26	0.08	1.79	0.10	0.91	0.03
11/03	0.14	0.03	1.40	0.09	0.97	0.02
11/04	0.20	0.03	1.74	0.07	0.94	0.04
11/05	0.25	0.03	1.57	0.05	0.96	0.04
11/12	0.03	0.01	1.31	0.12	0.94	0.06
11/13	0.08	0.01	1.66	0.07	0.97	0.03
11/16	0.14	0.03	1.24	0.15	0.98	0.03
11/18	0.11	0.00	0.58	0.00	0.99	0.00
11/23	0.19	0.02	1.33	0.19	0.97	0.02
11/29	0.05	0.01	1.34	0.07	0.97	0.02
12/01	0.10	0.02	1.32	0.09	0.94	0.01
12/04	0.17	0.01	1.22	0.02	0.93	0.03
12/06	0.07	0.01	0.95	0.12	0.88	0.05
12/08	0.07	0.01	1.18	0.11	0.93	0.06
12/09	0.06	0.02	0.75	0.16	0.87	0.08
12/10	0.20	0.00	0.99	0.00	0.87	0.00
12/12	0.10	0.01	1.24	0.05	0.89	0.08
12/13	0.10	0.01	0.78	0.06	0.99	0.01
12/14	0.06	0.01	1.05	0.13	0.86	0.08
12/18	0.12	0.02	1.31	0.12	0.95	0.03
12/19	0.06	0.00	0.69	0.13	0.96	0.04
12/24	0.16	0.01	1.44	0.09	0.90	0.05
12/26	0.18	0.01	0.88	0.01	0.96	0.03
12/29	0.08	0.01	1.32	0.02	0.92	0.02
12/30	0.05	0.00	1.01	0.10	0.85	0.06
12/31	0.08	0.01	1.20	0.05	0.91	0.04

Table S3. The average values of Absorption Ångström exponent (AAE) and the scattering Ångström exponent (SAE) at λ = 400 -675 nm with AOD > 0.2 during the summer, transition, and autumn period.

Summer		Transition		Autumn	
AAE	**SAE**	**AAE**	**SAE**	**AAE**	**SAE**
1.15 ± 0.84	1.25 ± 0.22	0.78 ± 0.47	1.13 ± 0.06	2.45 ± 0.91	1.46 ± 0.15

Table S4. The average (Avg.) values with the standard deviation (Std.) of the single scattering albedo (SSA) at each wavelength (λ) with AOD > 0.2 during the summer period.

Date (MM/DD)	SSA in Summer									
	λ = **400 nm**		λ = **500 nm**		λ = **675 nm**		λ = **870 nm**		λ = **1020 nm**	
	Avg.	**Std.**	**Avg.**	**Std.**	**Avg.**	**Std.**	**Avg.**	**Std.**	**Avg.**	**Std.**
07/20	0.96	0.02	0.97	0.01	0.94	0.02	0.99	0.01	0.99	0.01
07/30	0.95	0.01	0.97	0.01	0.94	0.01	0.99	0.01	0.99	0.01
08/05	0.96	0.02	0.97	0.02	0.99	0.01	0.92	0.06	0.98	0.02
08/06	0.97	0.01	1.00	0.00	1.00	0.00	1.00	0.00	1.00	0.00
08/12	0.97	0.04	0.98	0.04	0.98	0.05	0.94	0.06	0.94	0.08
08/20	0.99	0.01	0.99	0.01	0.99	0.01	0.99	0.01	0.98	0.02
08/21	0.94	0.03	0.98	0.02	0.98	0.02	0.99	0.01	0.96	0.04

Table S5. The average (Avg.) values with the standard deviation (Std.) of the single scattering albedo (SSA) at each wavelength (λ) with AOD > 0.2 during the autumn period.

Date (MM/DD)	SSA in Autumn									
	λ = **400 nm**		λ = **500 nm**		λ = **675 nm**		λ = **870 nm**		λ = **1020 nm**	
	Avg.	**Std.**	**Avg.**	**Std.**	**Avg.**	**Std.**	**Avg.**	**Std.**	**Avg.**	**Std.**
10/17	0.91	0.05	0.92	0.05	0.97	0.04	0.91	0.07	0.93	0.08
10/18	0.94	0.03	0.91	0.05	0.96	0.04	0.90	0.07	0.93	0.07
10/26	0.95	0.03	0.95	0.04	0.98	0.03	0.96	0.04	0.92	0.08
11/01	0.87	0.02	0.91	0.03	0.93	0.04	0.90	0.05	0.90	0.08
11/04	0.89	0.05	0.94	0.04	0.94	0.04	0.94	0.05	0.92	0.07
11/05	0.95	0.04	0.96	0.04	0.97	0.04	0.98	0.03	0.97	0.03
11/06	0.94	0.02	0.95	0.02	0.98	0.02	0.98	0.02	0.97	0.03